

Article

Decorating of Ag and CuO on ZnO Nanowires by Plasma Electrolyte Oxidation Method for Enhanced Photocatalytic Efficiency

Phung Thi Thu ², Vu Duy Thinh ^{3,4}, Vu Dinh Lam ⁴, Ta Ngoc Bach ¹, Le Thi Hong Phong ¹, Do Hoang Tung ⁵, Do Hung Manh ¹, Nguyen Van Khien ⁶, Trinh Xuan Anh ⁷ and Ngo Thi Hong Le ^{1,4,*}

¹ Institute of Materials Science, Vietnam Academy of Science and Technology, 18 Hoang Quoc Viet, Cau Giay, Hanoi 100000, Vietnam; bachtn.ims@gmail.com (T.N.B.); lephong.ims@gmail.com (L.T.H.P.); manhdh@ims.vast.ac.vn (D.H.M.)

² University of Science and Technology of Hanoi, Vietnam Academy of Science and Technology, 18 Hoang Quoc Viet, Cau Giay, Hanoi 100000, Vietnam; thuphungi2@gmail.com

³ Hanoi University of Mining and Geology, 18 Pho Vien, Dong Ngac, Bac Tu Liem, Hanoi 100000, Vietnam; vuduythinhbkk@gmail.com

⁴ Graduate University of Science and Technology, Vietnam Academy of Science and Technology, 18 Hoang Quoc Viet, Cau Giay, Hanoi 100000, Vietnam; lamvd@gust-edu.vast.vn

⁵ Institute of Physics, Vietnam Academy of Science and Technology, 18 Hoang Quoc Viet, Cau Giay, Hanoi 100000, Vietnam; dhtung@gmail.com

⁶ TNU-Thai Nguyen University of Sciences, Tan Thinh Ward, Thai Nguyen City 250000, Vietnam; khiennv@tnu.edu.vn

⁷ Hanoi University of Technology, 1 Dai Co Viet, Hanoi 100000, Vietnam; trinxuananh@gmail.com

* Correspondence: hongle@ims.vast.ac.vn or hongle2009@gmail.com



Citation: Thu, P.T.; Thinh, V.D.; Lam, V.D.; Bach, T.N.; Phong, L.T.H.; Tung, D.H.; Manh, D.H.; Van Khien, N.; Anh, T.X.; Le, N.T.H. Decorating of Ag and CuO on ZnO Nanowires by Plasma Electrolyte Oxidation Method for Enhanced Photocatalytic Efficiency. *Catalysts* **2022**, *12*, 801. <https://doi.org/10.3390/catal12070801>

Academic Editors: Vincenzo Vaiano and Olga Sacco

Received: 11 January 2022

Accepted: 15 July 2022

Published: 21 July 2022

Publisher's Note: MDPI stays neutral with regard to jurisdictional claims in published maps and institutional affiliations.



Copyright: © 2022 by the authors. Licensee MDPI, Basel, Switzerland. This article is an open access article distributed under the terms and conditions of the Creative Commons Attribution (CC BY) license (<https://creativecommons.org/licenses/by/4.0/>).

Abstract: In this work, photocatalytic performance is divulged in the ternary CuO-Ag-ZnO nanowire synthesized via a two-step approach. The decoration of Ag and CuO nanostructures onto the surface of ZnO nanowires was simply carried out by using the plasma electrolytic oxidation method in a short time. The structure, size, morphology, and optical properties of as-prepared samples were characterized by X-ray diffraction, field-emission scanning electron microscopy, and spectrophotometry measurements. The diameters of Ag nanoparticles and ZnO nanoflowers are in the range of 5–20 nm and 20–60 nm, respectively. Within the first 15 min, methyl orange was decolorized 96.3 and 82.8% in the CuO-Ag-ZnO and Ag-ZnO, respectively, and there is only about 46.7% of that decomposed in pure ZnO. The CuO-Ag-ZnO shows a higher rate constant $k = 0.2007 \text{ min}^{-1}$ and a lower half-life time $t = 6.1 \text{ min}$ compared to Ag-ZnO and bare ZnO nanowires. The photo-reusability of the ternary nanostructures was estimated to be much outweighed compared to ZnO nanowires. Interestingly, the synergic incorporation between noble metal–semiconductor or semiconductor–semiconductor in the interfaces of Ag-CuO, Ag-ZnO, and CuO-ZnO expands the visible light absorption range and eliminates the photogenerated electron–hole recombination, resulting in a superior visible-light-driven photocatalyst.

Keywords: ZnO nanowires; photoluminescence; plasma electrolytic oxidation; photocatalysis; noble metal

1. Introduction

Photodegradation of organic pollutants based on semiconductor photocatalysts has attracted tremendous interest due to its great potential for environmental protection and sustainable development. Of the outstanding semiconductors, zinc oxide (ZnO) has been appreciated as one of the most promising photocatalysts because of its superior properties, typically environmental friendliness, high chemical stability, inexpensiveness, high electron mobility, a large exciton binding energy (60 meV) at room temperature and excellent photocatalytic performance [1–4]. Furthermore, owing to high aspect ratio and

carrier transport, excellent interconnectivity and surface defect [5–9], one-dimensional (1D) nanostructured ZnO such as nanowires [8], nanofibers [10], and nanorods [9], combined with the advances in nanomaterial fabricating technology, have contributed to pushing up the further practical possibility of the ZnO materials. Nevertheless, disadvantages, i.e., a direct wide bandgap energy (3.3 eV) leading to narrow light response, fast photogenerated electron–hole recombination rate, and photo-instability in aqueous solution [1,4], result in poor light-harvesting and photocatalytic efficiencies.

To address these limitations, much consecutive effort has therefore been put forward to extend the light absorption region and enhance the charge separation efficiency. In this regard, one of the great strategies is to decorate noble metals like Au, Ag, and Pt onto the ZnO nanostructures [11–16]. It has been reported that the surface plasmon resonance property of noble metal nanoparticles efficiently improves the ZnO photocatalytic activity. In addition, coupling to other narrow band-gap semiconductors is also an efficient solution because the formation of p–n heterojunction at interfaces remarkably promotes the photogenerated carrier separation [17–19]. Moreover, visible-light-driven photocatalysts based on ternary noble metal/semiconductor/semiconductor structures have recently been studied as well [20–23]. A faster electron transfers rate and suppressed electron–hole recombination process are revealed in these heretofore structures [20,21]. Xu et al. reported that an Ag/CuO/ZnO nanotube film indicated enhanced photocatalytic activity and higher photostability with about 98% of photodegradation efficiency after 20 usage cycles [5].

Meanwhile, to the best of our knowledge, the evolution and elucidation of the photocatalytic enhancement mechanism in the semiconductor/noble metal/semiconductor structure is still very limited and has not met the practical requirements yet. Typically, Ren et al. reported a good photodegradation of methyl orange under the assistance of a ZnO/Au/Cu₂O structure [24]. In another work, ZnS and Ag were loaded onto the ZnO to form the ternary ZnS–Ag–ZnO for the aim to azo dye degradation under UV light. It was found that the ZnS–Ag–ZnO operated more efficiently than Ag–ZnO, commercial ZnO, and P25 [25]. Unfortunately, the rate constant has been a shortcoming for the ternary material system. Therefore, much more attention is indispensable in order to deal with this bottleneck. On the other hand, suitable component selection is a pivotal solution to construct an excellently photocatalytic ternary system. Comparing to Au, the work function of Ag nanostructure is in the vicinity of that of semiconductors, typically ZnO. Therefore, as participating in the ternary system, the Ag has been expected to bring out better responses. Gavade et al. made a comparison and indicated that the rate constant of Ag–Cu_xO–ZnO is higher than that of Au–Cu_xO–ZnO [26]. In addition, a p-type CuO semiconductor has received more attention for synthesizing CuO/ZnO heterostructure photocatalysts [27–30] owing to a narrow direct band gap in the range 1.2–1.5 eV, which favor the formation of p–n junction potential [31]. Noticeably, the emergence of an intrinsic electric field at the interfaces can eliminate the electron–hole recombination since CuO and ZnO have opposite charges. Consequently, the photogenerated electrons flow into the negative electric field and the corresponding holes flow into the positive field, giving rise to more efficient charge separation [31].

Decorating nanostructures onto the ZnO has been successfully realized by a variety of methods such as hydrothermal, electrodeposition, and sputtering [24–26,32]. For instance, ZnO/Au@Cu₂O was synthesized by hydrothermal method for many hours [32]. However, the majority of methods have consumed synthesizing time, extra supporting chemicals, or used complex techniques. Recently, advances in nanomaterial preparing techniques under plasma assistance have paved the way for a superior approach. The advantages that the method brings out consist of simplicity, short preparing time (several minutes), efficiency, and undestroyed backbone materials. Furthermore, the plasma method can be regarded as a “green” method, as it usually does not use auxiliary reagents in the synthesis process. As another benefit, this method can be carried out at ambient temperature and pressure.

Therefore, for the aim to further optimize the photocatalytic performance, in this work, we designed a novel nanowire ternary heterostructure, in which the Ag nanoparticles (NPs)

and CuO nanoflowers (NFs) were in turn anchored onto the surface of ZnO NWs and Ag NPs are covered by CuO NFs. It means that the noble metal Ag NPs are sandwiched by the n-type ZnO and the p-type CuO semiconductors in an encapsulated form. The formation of the interfacial electric field in the semiconductor–metal–semiconductor encapsulated structure was demonstrated to cause excellent photocatalytic efficiency. This nanowire ternary heterostructure was fabricated using the plasma electrolytic oxidation (PEO) treatment in several minutes. Meanwhile, it is worth mentioning that analogous heterostructures have been fabricated by more complicated approaches [24–26,32]. The match between the band structure energies of CuO, ZnO and Ag nanoparticles (NPs) are located between them, resulting in the establishment of a heterojunction that separates more efficiently the electron–hole pairs. Along with expanding the visible light absorption range, under the synergy of Ag and CuO, the CuO–Ag–ZnO has indicated an excellent photocatalyst working under the sunlight accompanied with a high rate constant k and a low half-life time. Its dye photodegradable activity significantly enhances compared to Ag–ZnO, bare ZnO, and other ternary structures reported [24,25]. Not only does the CuO–Ag–ZnO possess the highest photocatalytic efficiency, but its reusability is also more outstanding. Furthermore, the photoluminescence (PL) spectrum properties and the enhanced photocatalytic mechanism will be unraveled in the next section.

2. Results and Discussion

The size and morphological features of the pure ZnO, Ag–ZnO, and CuO–Ag–ZnO NWs were characterized by FE-SEM technique. Figure 1a presents the surface structure of the pure ZnO NWs obtained after a 3 h-hydrothermal process under reasonable conditions. The nanowires with smooth surfaces have diameters in the range of ~20–70 nm and a length of ~1–1.5 μm . Figure 1b,c shows the FE-SEM images of ZnO NWs decorated by Ag nanoparticles, and Ag and CuO nanoparticles, respectively, using the plasma electrolytic oxidation, which is simple and can be prepared in a short time (several minutes) [14,33]. Compared with the bare ZnO NWs, the successful deposition of the nanoparticles onto the surface of ZnO NWs can be confirmed. The Ag NPs with diameters from 5 to 20 nm are well dispersed on the ZnO NWs. Considerably, the emergence of flower-shaped CuO nanoparticles on the Ag–ZnO NWs, as shown in Figure 1c, points out the co-existence of the two types of nanoparticles. The diameter of CuO nanoflowers (NFs) grows in the range from 20 to 60 nm. Meanwhile, the CuO nanoflower sizes have been reported from several hundreds of nanometers to micrometers using chemical and time-consuming techniques like hydrothermal, wet chemical, and precipitation methods [34–36]. Consequently, the nanoflower sizes prepared here indicate superior advantages of PEO method compared to others.

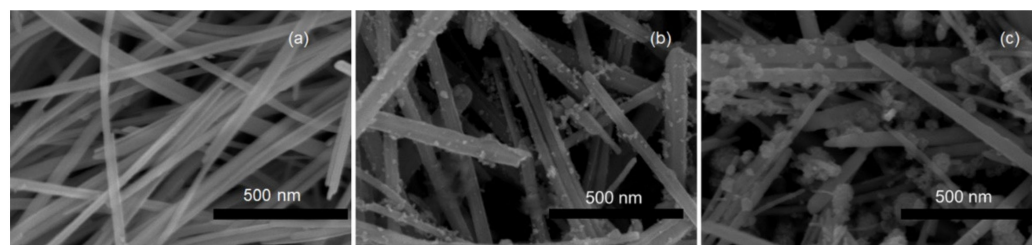


Figure 1. Morphologies of ZnO (a), Ag–ZnO (b), and CuO–Ag–ZnO (c) nanowires.

To get further analysis about the structural features of the as-prepared samples, TEM and HRTEM were used. In this regard, the CuO–Ag–ZnO sample was selected to reveal in detail the characteristics of Ag and CuO NPs onto the ZnO NWs. Figure 2 depicts TEM and HRTEM images of CuO–Ag–ZnO NWs. The resulting TEM images indicate the occupation of Ag NPs and CuO NFs onto the surface of nanowires. It can be deduced that the ZnO NWs acted as a substrate to support the formation and growth of Ag NPs and CuO NFs. A careful analysis of the HRTEM image (Figure 2b) confirmed the co-existence of lattice

fringes of ZnO, Ag, and CuO. The d-spacing of 0.24 nm, 0.24 nm, and 0.25 nm in lattice fringes corresponded to the (101) plane of ZnO NWs, the (111) plane of fcc-structure of Ag NPs, and the (111) plane of monoclinic CuO NFs. Note that the distribution of Ag NPs onto the surface of ZnO NWs operates as a key factor for decorating subsequent CuO NFs onto the NWs, whereas the nanoflowers were preferred to occupy the NWs with fewer Ag NPs.

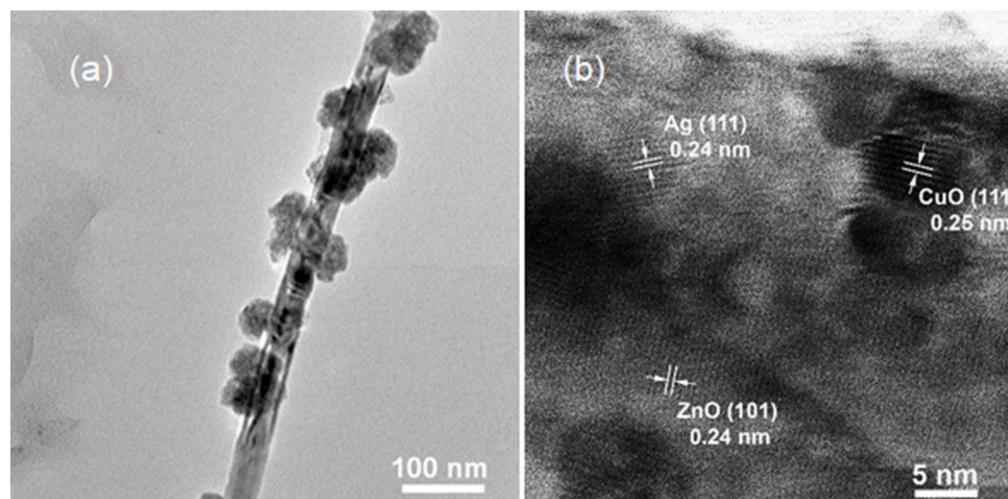


Figure 2. TEM (a) and HRTEM (b) images of CuO-Ag-ZnO nanowires.

The crystalline structure and phase composition of all samples were characterized by X-ray diffraction. Figure 3 shows the XRD pattern of pure ZnO, Ag-ZnO, and CuO-Ag-ZnO NWs. All the sharp peaks can be well indexed to the hexagonal wurtzite structure of the ZnO (JCPDS: 36-1451). Generally, characteristic diffraction peaks of ZnO NWs with the growth orientation along the c-axis are observed on all samples. The diffraction peaks located at 31.9° , 34.5° , 36.4° , 47.66° , 56.69° , and 63.1° can be assigned to the (111), (002), (101), (102), (110), and (103) crystal planes of the typical ZnO wurtzite crystal structure. No peak shift indicated that the Ag NPs and CuO NFs as well as the plasma treatment did not ruin the ZnO crystalline structure. To observe explicitly small diffraction peaks of Ag and CuO, a magnified portion of the XRD patterns in this range of $37\text{--}46^\circ$ was plotted in Figure 3. The presence of two peaks at 38.4 and 44.6° points to the existence of Ag NPs in the Ag-ZnO sample, corresponding to the (111) and (002) planes (matched with JCPDS: 04-0783), respectively. In the CuO-Ag-ZnO sample, the two characteristic peaks of metallic silver at 38.4 and 44.6° still exist, remarkably, the intensity of the peak at 38.4° increases two-fold, while that of the peak at 44.6° is unchanged. These further suggested that the CuO was attached on the Ag-ZnO NRs, corresponding to the (111) plane of monoclinic CuO (JCPDS: 05-0661). Therefore, it can be robustly concluded that the Ag and CuO were successfully decorated on the surface of ZnO NWs by the PEO without collapsing the ZnO crystal.

Figure 4 shows the Fourier transform infrared spectroscopy (FTIR) of the pure ZnO, Ag-ZnO and CuO-Ag-ZnO in the range of $400\text{--}4000\text{ cm}^{-1}$. The absorption peaks at 3445 cm^{-1} and 1632 cm^{-1} have been attributed to the O-H stretching and bending modes of chemisorbed water [26]. The peaks at 2917 cm^{-1} and 2855 cm^{-1} could be assigned to the C-H stretching vibrations. The additional peaks observed at 1368 cm^{-1} and 1060 cm^{-1} correspond to the C-O and C=O vibration modes, which may be due to carbonate group improper decomposition [26].

In general, the absorption bands below 1000 cm^{-1} correspond to the emergence of metal-oxide materials owing to the inter-atomic vibrations. The peaks appearing at $\sim 410\text{ cm}^{-1}$, 536 cm^{-1} and 540 cm^{-1} could be attributed to the metal-oxygen (M-O) (M=Zn, Cu) stretching vibration modes. From the Ag-ZnO curve in Figure 4, the absorption band of stretching of Zn-O can be observed between 536 cm^{-1} and 540 cm^{-1} , which confirms the

formation of the wurtzite structure of ZnO. The peaks at 410 cm^{-1} and $\sim 540\text{ cm}^{-1}$ could be assigned to the absorption of Cu-O, confirming the monoclinic structure of CuO [26,28].

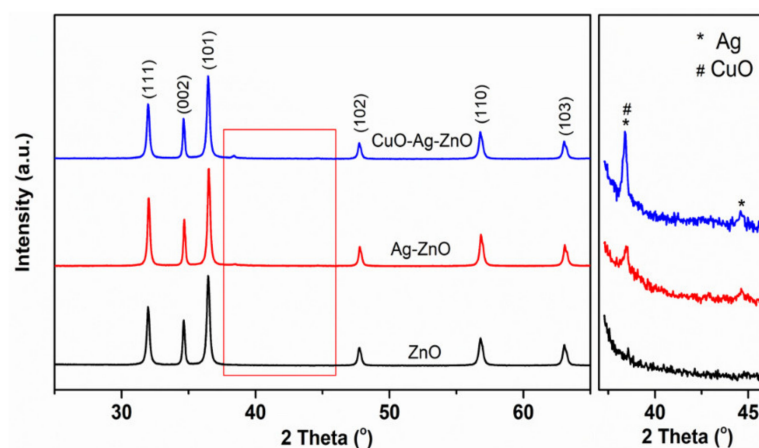


Figure 3. XRD diffraction patterns of as-prepared samples.

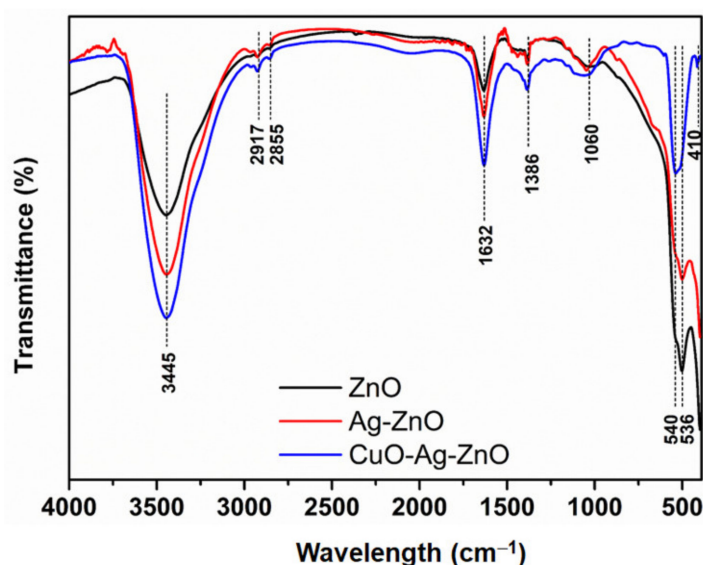


Figure 4. Fourier transform infrared (FTIR) spectra of samples.

We next discuss typical optical properties for as-prepared samples. Figure 5a introduces the optical absorption spectra of the pure ZnO, Ag-ZnO, and CuO-Ag-ZnO NWs. Obviously, the absorption edge of Ag-ZnO NWs is nearly unchanged compared to pure ZnO NWs. However, the change occurs at the absorptive intensity in the visible light region from approximately 400 nm to 550 nm. This can be attributed to the localized energy states in the band gap of ZnO NWs due to the formation of defects in the ZnO lattice during Ag decoration as well as the localized surface plasmon resonance (LSPR) effect by Ag NPs [37]. When a narrow band gap semiconductor CuO (1.4 eV [38]) coupling with Ag-ZnO gives rise to suppressing the recombination process because it absorbs the visible part of the incident light and also supports the electron transfer to the large band gap semiconductor (ZnO). The absorption edge of the CuO NF- decorated Ag-ZnO NWs is red-shifted compared to Ag-ZnO NWs and ZnO NWs. This leads to a greatly enhanced absorbance in the visible light region and is quite beneficial for harvesting the light and producing more photogenerated charge carriers. This shift in the absorption wavelength also confirms the formation of CuO-Ag-ZnO heterojunction.

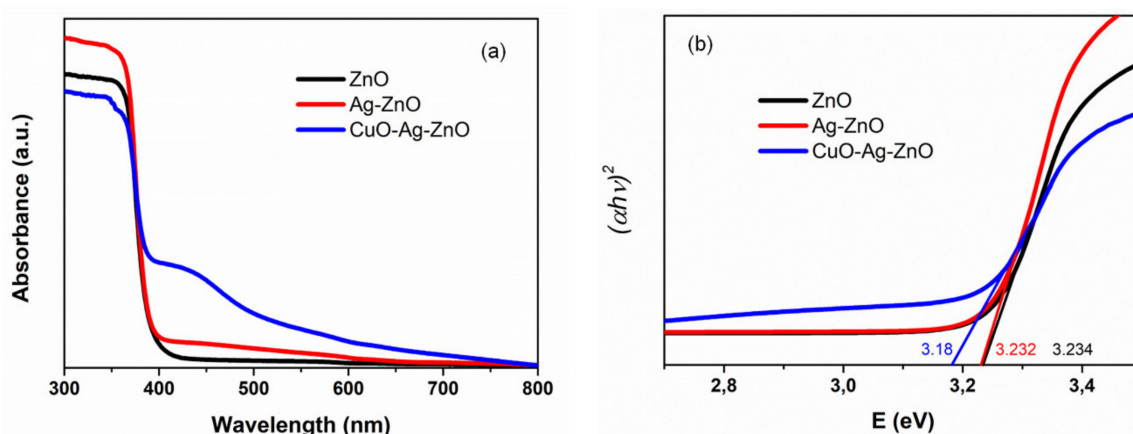


Figure 5. Absorbance spectra of samples (a), and Tauc plot for calculation of bandgap of samples (b).

Since ZnO exhibits a direct bandgap at ambient conditions [39], Tauc model was used to define the bandgap of as-prepared samples, given in the following equation:

$$\alpha h\nu = A(h\nu - E_g)^n. \quad (1)$$

where A is constant, h is Planck's constant, ν is the photon frequency, E_g is the optical bandgap, and $n = 1/2$ for the direct bandgap semiconductor. By extrapolating the linear region of $(\alpha h\nu)^2$ versus the photon energy axis, the optical band gaps were estimated as shown in Figure 5b. It clearly shows that the pure ZnO and Ag-ZnO NWs get nearly the same band gap of ~ 3.23 eV. Nevertheless, the band gap of CuO NF-decorated Ag-ZnO NWs shifts to ~ 3.18 eV. Accordingly, it can be concluded that the formation of CuO NFs can narrow the band gap energy of Ag-ZnO NWs.

Figure 6 shows the room-temperature PL spectra of ZnO, Ag-ZnO, and CuO-Ag-ZnO NWs. As well-known, the PL spectra of ZnO have a near band-gap emission (NBE), 380–390 nm, which can be regarded as the free excitonic (electron–hole pair) recombination, and a deep level emission (DLE) originates from the defect levels [40]. The ultra-violet (UV) PL intensities of Ag-ZnO NWs and CuO-Ag-ZnO NWs are about a 1.4-fold increase and 3-fold decrease compared to the bare ZnO NWs, respectively. The visible (VIS) PL intensities of Ag-ZnO NWs and CuO-Ag-ZnO NWs are about a 3.1-fold and 5.5-fold decrease compared to the ZnO NWs, respectively. The enhancement or quenching of the PL emission strongly depends on the band structures of the semiconductor and the metal as well as the emission energy states, and the direction of the energy or electron transfers between the metal NPs and semiconductors [41]. The enhancement in the UV PL emission of Ag-ZnO NWs can stem from the coupling between the excitons in the ZnO NWs and the LSPR in Ag NPs, discussed in detail in Ref. [14]. The energy or electron transfer from the Ag NPs to the semiconductor ZnO and the PL emission can be enhanced. However, the VIS PL intensity of Ag-ZnO NWs significantly decreases compared to that of ZnO NWs. This behavior may be due to the matching between the visible emission energy of ZnO and the LSPR energy of Ag NPs, and the energy or electron transfer from metal to the defect level of ZnO. These electrons can be easily excited to the conduction band, giving rise to the reduction of the recombination between the electrons and the holes. Consequently, the visible emission of Ag-ZnO is lower than that of the ZnO, and hence the photocatalytic activity of Ag-ZnO can be enhanced, as also suggested previously [42]. As expected, in synthesized samples, the PL intensity of CuO-Ag-ZnO NWs is the lowest, which means that the electron–hole separation efficiency is highest. In this hetero-composite, the interaction of two semiconductors with noble metal nanoparticles results in the establishment of the Ag-ZnO, and Ag-CuO heterojunction interfaces. In addition, the work functions of CuO, ZnO, and Ag NPs are located at -4.07 eV, -4.35 , and -4.26 eV in terms of the absolute vacuum scale, respectively [43,44]. As seen in Figure 7, under the UV-VIS light, the electrons

in CuO excited from the valance band to the conduction band can transfer to the Fermi level of Ag NPs and the ZnO conduction band. Electrons from the Fermi level can also move into the conduction band of ZnO. As a consequence, the decrease of the PL intensity at both the UV and VIS emissions is rendered, leading to a noteworthy suppression in the electron–hole recombination rate and thus the prominent improvement of photocatalytic degradation of catalysts.

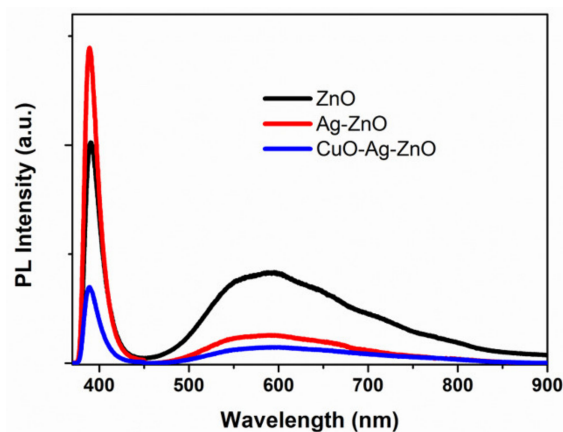


Figure 6. PL spectra of as-prepared samples.

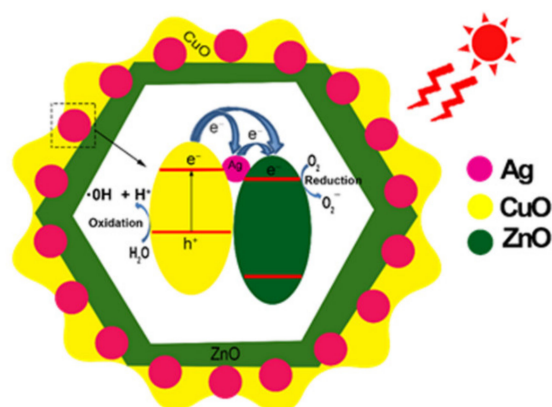


Figure 7. A schematic band diagram for electron transfer between the conduction band of CuO, ZnO, and the Ag Fermi level.

As well-known, the electron and hole separation efficiency in the semiconductors has a great influence on photocatalytic activity. Figure 8a shows the photocurrent-time curves of ZnO, Ag-ZnO, and CuO-Ag-ZnO photoelectrodes under the light on/off illumination by the solar simulated light. It can be seen explicitly that the CuO-Ag-ZnO points out a significantly increased photocurrent, compared to that of the ZnO and Ag-ZnO. The enhancement of photocurrent density in the CuO-Ag-ZnO indicates the separation efficiency of photogenerated carriers, which can be accountable for its high photocatalytic activity [45,46] because of our ternary nanostructure. In addition, the electrochemical impedance spectroscopy (EIS) can be considered as a powerful tool to estimate charge separation/transfer and recombination processes in photocatalysts. Figure 8b illustrates the Nyquist plot of ZnO, Ag-ZnO and CuO-Ag-ZnO. The radius of the arc on the Nyquist plot represents the interface layer resistance occurring at the surface of the electrode. The arc radius on EIS Nyquist plot of the CuO-Ag-ZnO is smaller than that of the ZnO and Ag-ZnO. It suggests that the ternary CuO-Ag-ZnO has more effective charge separation and faster interfacial charge transfer. These results indicate that the decoration of Ag NPs and especially CuO NFs onto the ZnO NWs can effectively improve the photogenerated charge separation [45,46]. In addition, these results may be attributed to the interfacial

electric field between ZnO and Ag NPs in Ag-ZnO NW samples as well as the ZnO, Ag and CuO in the CuO-Ag-ZnO NWs, which accelerates the migration of photogenic charges under UV-VIS light [47].

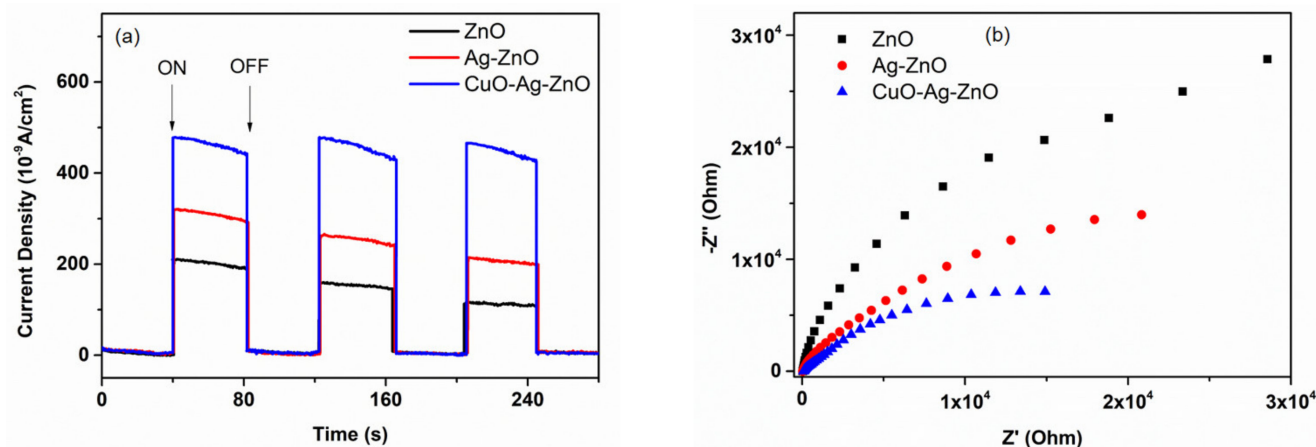


Figure 8. (a) The photocurrent-time curves of samples under the light on/off illumination by the solar simulated light, and (b) the Nyquist plot of samples.

The photocatalytic activities of the ZnO, Ag-ZnO and CuO-Ag-ZnO NWs were evaluated with respect to the degeneration of methyl orange (MO) dye under the solar simulator light. Photogenerated electrons in the conduction band can capture oxygen to form superoxide anion radicals ($\cdot\text{O}^{-2}$) while corresponding holes in the valence band can react with H_2O to form hydroxyl radicals ($\cdot\text{OH}$), both of which serve as pivotal factors for the dye degradation. The photodegradable process was investigated by monitoring the change in the maximum absorption peak of MO dye at 465 nm. Figure 9 manifests the UV-vis absorption spectra of MO in terms of irradiation time for ZnO, Ag-ZnO, and CuO-Ag-ZnO NWs. The intensity of absorption spectra, in general, markedly reduced upon increasing the irradiation time. It can be seen that when the irradiation time increases, the peak position is shifted to the left, due to the formation of the intermediate products after the degradation of the MO dye.

Figure 10a shows the relationship between C_t/C_0 degradation and irradiation times, where C_t is the MO concentration at time t and C_0 is the initial concentration, which derives the decolorization efficiency (%). The CuO-Ag-ZnO NWs obviously have the highest photocatalytic activity, and about 100% of MO could be degraded within 30 min of solar simulator irradiation. The Ag-ZnO, and ZnO NWs have lower photocatalytic activity, in which about 98.5 and 89% of MO were photo-decomposed within 30 min, respectively. It is worth mentioning that within the first 15 min, the CuO-Ag-ZnO NWs degrade about 96.3% of MO dye, while the lower decolorization efficiency is observed in the Ag-ZnO NWs and ZnO NWs with about 82.8 and 46.7%, respectively. Thus, the photocatalytic activity of the CuO-Ag-ZnO NWs is greatly improved due to the contribution of the decoration of Ag NPs and CuO NFs onto the ZnO NW surface. These results are in consistence with the PL spectra mentioned above. To evaluate the reaction kinetics of the MO photodegradation of all samples, the experimental data in Figure 10b were fitted by the Langmuir-Hinshelwood equation: $\ln(C_0/C_t) = kt$, where k is a pseudo-first-rate kinetic constant and t is the irradiation time. By the approximate linear fitting curves of $\ln(C_0/C_t)$ versus irradiation time t , the values of k of ZnO, Ag-ZnO, and CuO-Ag-ZnO NWs were calculated to be 0.05 min^{-1} , 0.135 min^{-1} , and 0.2007 min^{-1} , respectively. Noticeably, the value k of CuO-Ag-ZnO NWs was estimated to be larger than that of previous reports. Munawa et al. [44] reported that the rate constant of ZnO-CdO-CuO nanocomposite for the degradation of MO is only 0.01964 min^{-1} . Ren et al. [24] fabricated ternary ZnO@Au@Cu₂O nanorod films by the electrodeposition and a sputtering method. They claimed that the rate constant for degradation of MO is 0.3027 h^{-1} . In another work, Ren et al. [45] also found that the rate

constant of ZnO@Au@Cu₂O nanorod films for the degradation of MO is about 0.35 h⁻¹. The fundamental mechanism for the photocatalytic enhancement in our sample can be explained due to (1) work function of Ag (-4.26 eV), ZnO (-4.35 eV), CuO (-4.07) is quite close, and (2) the simultaneous existence heterojunction in the CuO-Ag-ZnO NWs.

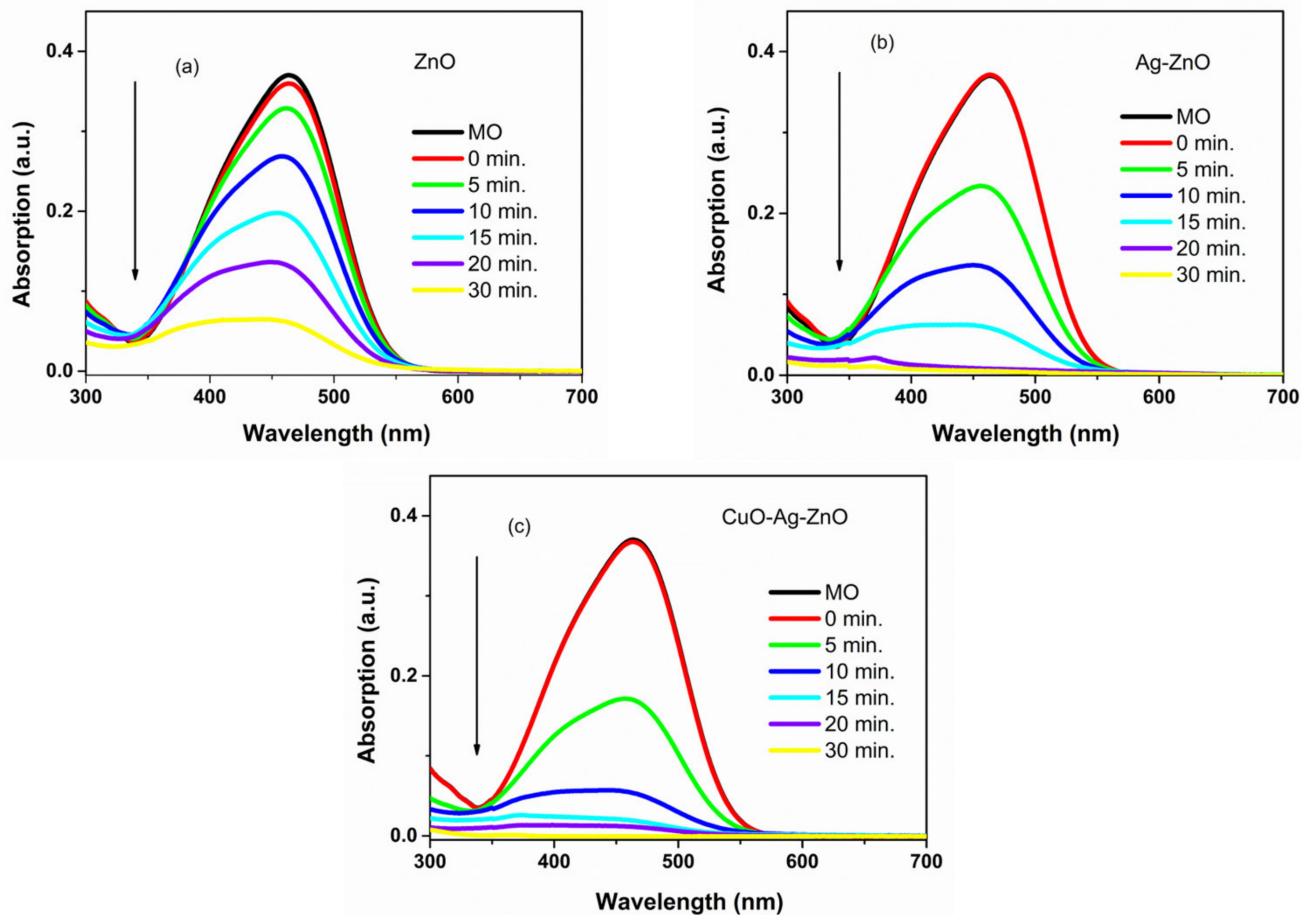


Figure 9. UV-vis absorption spectra of ZnO (a), Ag-ZnO (b), and CuO-Ag-ZnO (c) for degradation of MO under irradiation of solar simulator light by the as-prepared samples.

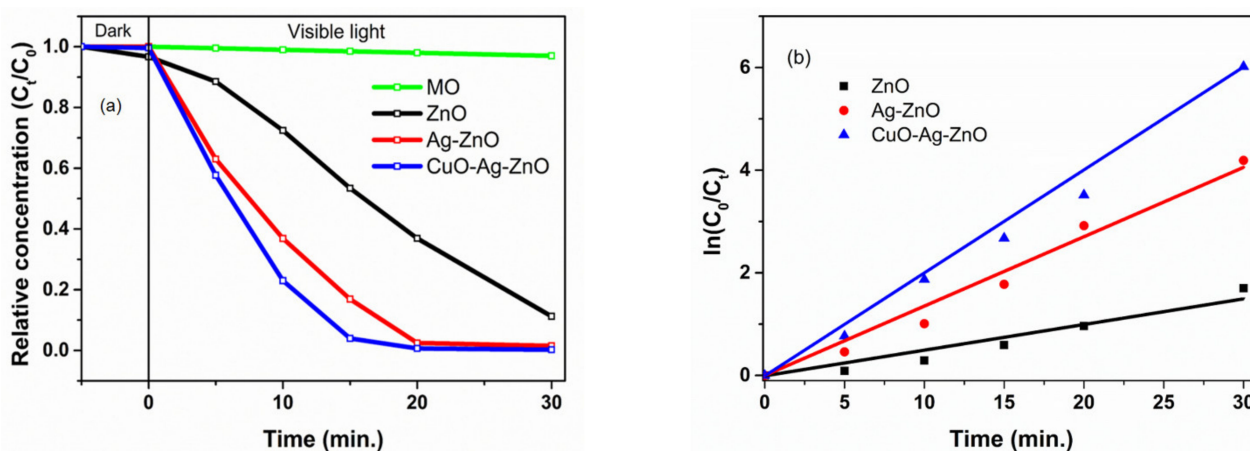


Figure 10. (a) Kinetics of MO photodegradation by the prepared samples, and (b) $\ln(C_0/C_t)$ curve as a function of time for the photodegradation process of MO.

The synthesis time and the photocatalysis rate constant for MO dye of CuO-Ag-ZnO are compared with those of other photocatalyst composites reported in the literature, as

listed in Table 1. It can be clearly seen that the synthesis time and the photocatalysis rate constant of CuO-Ag-ZnO are shorter and higher than those of other photocatalyst composites, respectively. Therefore, such CuO-Ag-ZnO NWs could be considered as excellent photocatalysts for the degradation of MO dye.

Table 1. A comparative table of photodegradation of MO dye solutions.

Sr. No.	Catalyst Materials	Synthesis Routes	Synthesis Time	Light Source	* k	Ref.
01	Ag-CuO-ZnO NRs	Sol-gel method Photodeposition (Ag, CuO)	5 h 4 h	Xenon lamp (50 mW cm ⁻² , 420–720 nm)	~0.1 min ⁻¹	[5]
02	Ag-CuO-ZnO NTs	Sol-gel method Photodeposition (Ag, CuO)	5 h 4 h	Xenon lamp (50 mW cm ⁻² , 420–720 nm)	~0.3 min ⁻¹	[5]
03	ZnO@Au@Cu ₂ O	Electrochemical method Sputtering method (Au, Cu ₂ O)	1 h 60 s	Solar simulator (Bos-X350-Z, -AM, 60 mW/cm ²)	0.3 h ⁻¹	[24]
04	Ag@Cu _x O/ZnO	Milling method Reduction method (Ag, Cu ₂ O)	4 h 3 h	UV (365 nm)	18.06 × 10 ⁻² min ⁻¹	[26]
05	CuO-ZnO-Ag	Sol-gel method	-	UV-VIS	0.0885 min ⁻¹	[47]
06	(ZnO) _{0.2} /(Fe ₂ O ₃) _{0.6} /(CuO) _{0.2}	Hydrothermal (ZnO) Precipitation method (Fe ₂ O ₃) Hydrothermal (CuO)	1.5 h 2 weeks 1.5 h	Two tungsten halogen lamps (ASI Illuminator, 50 W each)	0.039 min ⁻¹	[48]
07	ZnO@Ag@Cu ₂ O	Electrochemical method Sputtering method (Au, Cu ₂ O)	1 h 60 s	Solar simulator (Bos-X350-Z, -AM, 60 mW/cm ²)	0.3 h ⁻¹	[49]
08	CuO-Ag-ZnO Present work	Hydrothermal (ZnO) Plasma electrolytic oxidation (PEO) treatment (CuO, Ag)	3 h 10 min.	Solar simulator (Oriel Sol1A, 100 mW cm ⁻²)	0.2007 min ⁻¹	

* k is a pseudo-first-rate kinetic constant.

The natural degradation is usually considered a half-life, by using CuO-Ag-ZnO NWs as the photocatalyst, the half-life of MO was estimated by the intersection between the curve of degradation efficiency ($1-C_t/C_0$) and dye concentration (C_t/C_0) versus irradiation time. The value of $t_{1/2}$ is found to be 6.1 min (Figure 11a). This half-life of CuO-Ag-ZnO NWs is much lower than that of composite samples in previous reports [47]. In addition to the photocatalytic activity, the stability and reusability of photo-catalytic materials are crucial factors for practical contaminated water treatment. It is noted that ZnO is known as an unstable photocatalyst in an aqueous environment [47]. This drawback is significantly overcome in our ternary structure. Typically, the CuO-Ag-ZnO NWs were used in the photodegradation of dye 20 times, and after each run, CuO-Ag-ZnO NWs were separated from the reaction mixture by centrifugation. The recovered catalyst was then reused to degrade MO to a fresh solution. Figure 11b shows the photocatalytic degradation of MO solution in 20 successive runs using ZnO, Ag-ZnO and CuO-Ag-ZnO NWs. There is no significant change in the degradation efficiency of CuO-Ag-ZnO NWs for MO after multiple cycles, while that of Ag-ZnO and ZnO NWs decrease 35 and 40%, respectively. As a result, the CuO-Ag-ZnO NWs exhibited higher stability and reusability. Therefore, the Ag NPs and CuO NFs play an important role in the augmentation of photodegradation efficiency, stability, and reusability of ZnO nanomaterials.

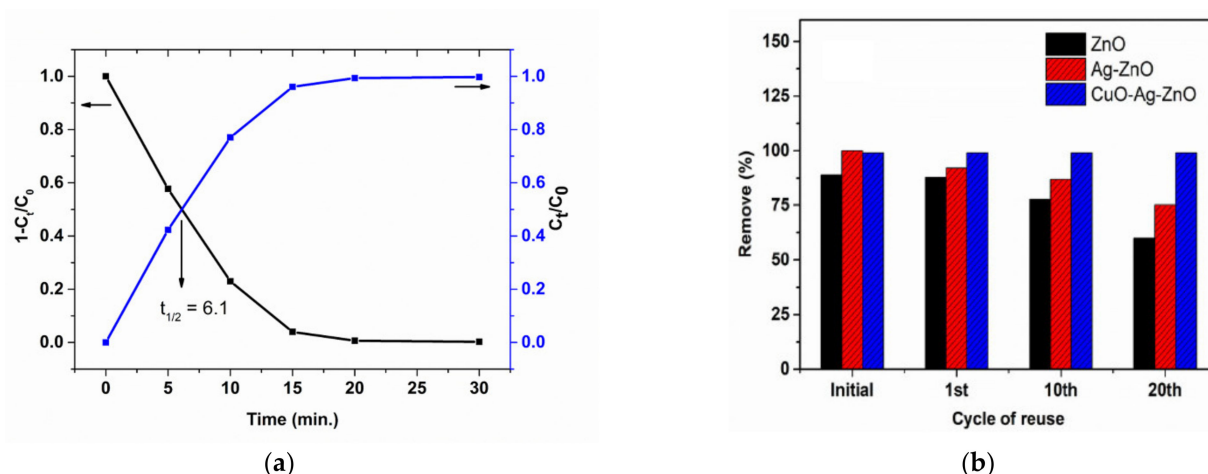


Figure 11. (a) Half-life estimation curve for degradation of MO dye using CuO-Ag-ZnO NWs, and (b) reuse studies of MO using ZnO, Ag-ZnO and CuO-Ag-ZnO.

3. Materials and Methods

3.1. Materials

All the chemicals used were of analytical grade. Zinc nitrate hexahydrate ($\text{Zn}(\text{NO}_3)_2 \cdot 6\text{H}_2\text{O}$), sodium carbonate (Na_2CO_3), silver nitrate (AgNO_3), copper (II) nitrate hydrate $\text{Cu}(\text{NO}_3)_2$, ammonium hydroxide solution (NH_4OH 25%), ascorbic acid ($\text{C}_6\text{H}_8\text{O}_6$), and ethanol ($\text{C}_2\text{H}_5\text{OH}$) were received from Sigma-Aldrich (St. Louis, MA, USA).

3.2. Synthesis of ZnO Nanowires

ZnO nanowires (NWs) were simply synthesized by the hydrothermal method at a moderate temperature of 120°C for 3 h. Particularly, a mixture consisting of $\text{Zn}(\text{NO}_3)_2 \cdot 6\text{H}_2\text{O}$ and Na_2CO_3 was dissolved well in distilled water for 1 h. This mixed solution was then transferred into a Teflon put in a steel autoclave to perform the hydrothermal process. The white powder was taken out and washed several times with distilled water and ethanol to remove un-reacted substances and impurities, and then dried at 70°C for 24 h.

3.3. Synthesis of Ag-ZnO and CuO-Ag-ZnO Nanowires

Decoration of silver on the ZnO NWs using the PEO process was presented in our previous reports [14]. The as-prepared ZnO powder was dispersed well in NH_4OH aqueous solution with $\text{pH} \sim 8$ using the ultrasonic device. The plasma was discharged into the above mixture for 3 min. Then, 50 mM AgNO_3 -precursor solution was introduced and continue discharging the plasma for 5 min. One obtained Ag-ZnO powder using centrifugation and washing 3 times with distilled water. Next, to fabricate ternary CuO-Ag-ZnO heterostructure, after Ag-ZnO synthesizing step, $\text{Cu}(\text{NO}_3)_2$ -precursor and ascorbic acid, via the molar ratio $\text{AgNO}_3:\text{Cu}(\text{NO}_3)_2:\text{ascorbic acid} = 1:63:8$, were dropped and the plasma treatment was realized for 10 min. CuO-Ag-ZnO powders were isolated using centrifugation for 5 min at 5800 rpm and washing several times with distilled water. These samples were dried in a vacuum oven for 24 h at 50°C and stored in a sealed vessel.

3.4. Sample Characterization

The surface morphology of the samples was observed by field emission scanning electron microscopy (FESEM, Hitachi, S4800). Their crystal structure was determined by a Bruker D8 advanced X-ray powder diffractometer with Cu-K α radiation ($k = 1.5406 \text{ \AA}$). FT-IR spectra were engaged via a Nicolet iS10 spectrometer (Thermo Scientific, Waltham, MA, USA). PL spectra of the ZnO samples were obtained by the excitation of a 355 nm Teem Photonic laser. The photoluminescence spectrum was measured by high-resolution photoluminescence spectroscopy (iHR550). The UV-vis absorption spectrum was examined by a UV-vis-NIR spectrophotometer Carry 5000 (Varian, Palo Alto, CA, USA).

3.5. Photoelectrochemical Experiments

Sample films were prepared on cleaned fluorine doped tin oxide (FTO) glass electrodes by doctor blade technique. In this experiment, a paste was made from as-prepared samples and a mixture of 20:1.3:1 ethanol, acetylacetone, and Triton X-100 non-ionic surfactant using milling method. The film area and thickness are about 1 cm² and 500 nm, respectively. The photoelectrochemical measurements were carried out with μ Stat-i 400s Potentiostat using a three-electrode system with a Pt wire as the counter electrode, Ag/AgCl as the reference electrode, and the as-prepared photoanodes as the working electrode at room temperature. Then, 0.25 M Na₂SO₄ aqueous solution was used as the electrolyte. Electrochemical impedance spectroscopy (EIS) was measured in the frequency range of 0.5 Hz–105 KHz, with an AC voltage amplitude of 10 mV. For the photocurrent responses over time (I–t curves), the working electrode was illuminated using the solar simulator irradiation (AM 1.5) with a power of 100 mW cm⁻² (Oriol Sol1A, Newport, Irvine, CA, USA) at 0.0 V versus Ag/AgCl.

3.6. Photocatalytic Test

The photocatalytic activity of the as-prepared samples, involving ZnO, Ag-ZnO, and CuO-Ag-ZnO, was estimated by means of the photodegradation of Methyl orange (MO) under the solar simulator irradiation (AM 1.5) with a power of 100 mW cm⁻² (Oriol Sol1A). Overall, 20 mg of each photocatalyst was conducted into 30 mL of MO (10 ppm) contained in a glass beaker (DURAN, Duisburg, Germany). This mixture was then stirred in the dark condition for one hour so that the photocatalyst's surface reached the adsorption-desorption equilibrium state. Subsequently, the incident light source was irradiated perpendicularly to the solution surface for 30 min. At every certain time interval, 3 mL of the solution was aspirated and put into a centrifuge tube. The UV-vis spectrophotometer was applied to measure the concentration of MO following the illuminative time.

4. Conclusions

To sum up, we successfully synthesized a novel ternary CuO-Ag-ZnO nanowire heterostructure in the semiconductor-metal-semiconductor encapsulated form via a two-step approach, whereas the ZnO NWs serving as host materials were formed by a facile hydrothermal treatment and the Ag NPs and CuO NFs were in turn anchored on the surface of ZnO NWs by a simple, fast and efficient PEO treatment. The diameters of Ag NPs and ZnO NFs are in the range of 5–20 nm and 20–60 nm, respectively. Under the UV-vis light, methyl orange was decolorized 96% in the CuO-Ag-ZnO, while there are about 83 and 47% of MO decomposed in the Ag-ZnO and bare ZnO NWs, respectively, in the first 15 min. Most prominently, the CuO-Ag-ZnO indicated a largely high photodegradable rate $k \sim 0.2 \text{ min}^{-1}$ (0.05 min^{-1} and 0.135 min^{-1} corresponding to ZnO and Ag-ZnO, respectively), and a lower half-life time $t_{1/2} \sim 6.1 \text{ min}$. In addition, it was found that the partial suppression of PL spectra at both UV and VIS emissions demonstrates the highest photocatalytic efficiency exhibited in the CuO-Ag-ZnO NWs in comparison to Ag-ZnO in which such behavior only occurs at the VIS emission while the UV emission is pushed up, and bare ZnO. These responses are attributed to primarily stem from the incorporation of Schottky barriers and p-n heterojunction effects at the Ag-ZnO, Ag-CuO, and CuO-ZnO interfaces. Consequently, along with photoelectrochemical measurement results, the most efficient photogenerated charge transfer and separation as well as enhanced visible light harvesting were ascribed in the CuO-Ag-ZnO NWs. Furthermore, its photo-reusability was also much more outweighed than that of bare ZnO and, therefore, paving the way for a great potential of ZnO-based ternary nanostructures for practically photocatalytic treatment and other applications.

Author Contributions: Conceptualization, N.T.H.L., P.T.T. and V.D.L.; methodology, N.T.H.L. and T.X.A.; validation, N.T.H.L., P.T.T., V.D.T. and N.V.K.; formal analysis, P.T.T., N.T.H.L. and T.N.B., V.D.T.; investigation, P.T.T., T.N.B., L.T.H.P., V.D.T. and D.H.T.; data curation, P.T.T., L.T.H.P., N.V.K.

and T.N.B.; writing—original draft preparation, P.T.T., D.H.M. and N.T.H.L.; writing—review and editing, N.T.H.L.; visualization, supervision, N.T.H.L., V.D.L. and D.H.M.; project administration, N.T.H.L.; funding acquisition, N.T.H.L. All authors have read and agreed to the published version of the manuscript.

Funding: This research was funded by the National Foundation for Science and Technology Development (NAFOSTED), grant number 104.03-2017.40.

Data Availability Statement: The data that support the plots within this paper are available from the corresponding author on reasonable request.

Conflicts of Interest: The authors declare no conflict of interest.

References

1. Ong, C.B.; Ng, L.Y.; Mohammad, A.W. A review of ZnO nanoparticles as solar photocatalysts: Synthesis, mechanisms and applications. *Renew. Sustain. Energy Rev.* **2018**, *81*, 536–551. [[CrossRef](#)]
2. Zhang, B.Q.; Dandeneau, C.S.; Zhou, Z.; Cao, G. ZnO nanostructures for dye-sensitized solar cells. *Adv. Mater.* **2019**, *21*, 4087–4108. [[CrossRef](#)]
3. Zhou, J.; Xu, N.; Wang, Z.L. Dissolving behavior and stability of ZnO wires in biofluids: A study on biodegradability and biocompatibility of ZnO nanostructures. *Adv. Mater.* **2006**, *18*, 2432–2435. [[CrossRef](#)]
4. Qi, K.; Cheng, B.; Yu, J.; Ho, W. Review on the improvement of the photocatalytic and antibacterial activities of ZnO. *J. Alloys Compd.* **2017**, *727*, 792–820. [[CrossRef](#)]
5. Xu, K.; Wu, J.; Tan, C.F.; Ho, G.W.; Wei, A.; Hong, M. Ag-CuO-ZnO metal-semiconductor multiconcentric nanotubes for achieving superior and perdurable photodegradation. *Nanoscale* **2017**, *9*, 11574–11583. [[CrossRef](#)] [[PubMed](#)]
6. Han, Z.; Li, Y.; Lin, X.; Wang, Z.; Li, Z.; Wang, H.; Zhu, L. Preparation and photoelectrocatalytic performance of Fe₂O₃/ZnO composite electrode loading on conductive glass. *Chem. J. Chin. Univ.* **2018**, *39*, 771–778.
7. Han, Z.; Li, Y.; Chen, F.; Tang, S.; Wang, P. Preparation of ZnO/Ag₂O nanofibers by coaxial electrospinning and study of their photocatalytic properties. *Chem. J. Chin. Univ.* **2020**, *41*, 308–316.
8. Pivet, M.L.; Poupart, R.; Capochichi-Gnambodoe, M.; Martin, N.; Leprince-Wang, Y. Direct growth of ZnO nanowires on civil engineering materials: Smart materials for supported photodegradation. *Microsyst. Nanoeng.* **2019**, *5*, 57. [[CrossRef](#)]
9. Zhang, X.; Qin, J.; Xue, Y.; Yu, P.; Zhang, B.; Wang, L.; Liu, R. Effect of aspect ratio and surface defects on the photocatalytic activity of ZnO nanorods. *Sci. Rep.* **2014**, *4*, 4596. [[CrossRef](#)]
10. Fang, X.; Li, S.; Wang, X.; Fang, F.; Chu, X.; Wei, Z.; Li, J.; Chen, X.; Wang, F. The growth and photocatalytic property of ZnO nanofibers synthesized by atom layer deposition using PVP nanofibers as templates. *Appl. Surf. Sci.* **2012**, *263*, 14–17.
11. Mauro, A.D.; Zimbone, M.; Scuderi, M.; Nicotra, G.; Fragalà, M.E.; Impellizzeri, G. Effect of Pt nanoparticles on the photocatalytic activity of ZnO nanofibers. *Nanoscale Res. Lett.* **2015**, *10*, 484. [[CrossRef](#)] [[PubMed](#)]
12. Deng, Q.; Duan, X.; Ng, D.H.L.; Tang, H.; Yang, Y.; Kong, M.; Wu, Z.; Cai, W.; Wang, G. Ag nanoparticle decorated nanoporous ZnO microrods and their enhanced photocatalytic activities. *ACS Appl. Mater. Interfaces* **2012**, *4*, 6030–6037. [[CrossRef](#)] [[PubMed](#)]
13. Trang, T.N.Q.; Phan, T.B.; Nam, N.D.; Thu, V.T.H. In situ charge transfer at the Ag@ZnO photoelectrochemical interface toward the high photocatalytic performance of H₂ evolution and RhB degradation. *ACS Appl. Mater. Interfaces* **2020**, *12*, 12195–12206. [[CrossRef](#)] [[PubMed](#)]
14. Thinh, V.D.; Lam, V.D.; Bach, T.N.; Van, N.D.; Manh, D.H.; Tung, D.H.; Lien, N.T.H.; Thuy, U.T.D.; Anh, T.X.; Tung, N.T.; et al. Enhanced optical and photocatalytic properties of Au/Ag nanoparticle-decorated ZnO films. *J. Electron. Mater.* **2020**, *49*, 2626–2632. [[CrossRef](#)]
15. He, W.; Kim, H.-K.; Wamer, W.G.; Melka, D.; Callahan, J.H.; Yin, J.-J. Photogenerated charge carrier and reactive oxygen species in ZnO/Au hybrid nanostructures with enhanced photocatalytic and antibacterial activity. *J. Am. Chem. Soc.* **2014**, *136*, 750–757. [[CrossRef](#)]
16. Li, X.Z.; Li, F.B. Study of Au/Au³⁺—TiO₂ photocatalysts toward visible photooxidation for water and wastewater treatment. *Environ. Sci. Technol.* **2001**, *35*, 2381–2387. [[CrossRef](#)]
17. Moon, G.D.; Joo, J.B.; Lee, I.; Yin, Y. Decoration of size-tunable CuO nanodots on TiO₂ nanocrystals for noble metal-free photocatalytic H₂ production. *Nanoscale* **2014**, *6*, 12002–12008. [[CrossRef](#)]
18. Zhang, S.; Gong, X.; Shi, Q.; Ping, G.; Xu, H.; Waleed, A.; Li, G. CuO nanoparticle-decorated TiO₂-nanotube heterojunctions for direct synthesis of methyl formate via photo-oxidation of methanol. *ACS Omega* **2020**, *5*, 15942–15948. [[CrossRef](#)]
19. Zhu, L.; Li, H.; Xia, P.; Liu, Z.; Xiong, D. Hierarchical ZnO decorated with CeO₂ nanoparticles as the direct Z-scheme heterojunction for enhanced photocatalytic activity. *ACS Appl. Mater. Interfaces* **2018**, *10*, 39679–39687. [[CrossRef](#)]
20. Zhao, S.; Cheng, Z.; Kang, L.; Li, M.; Gao, Z. The facile preparation of Ag decorated TiO₂/ZnO nanotube and their potent photocatalytic degradation efficiency. *RSC Adv.* **2017**, *7*, 50064–50071. [[CrossRef](#)]
21. Mulkhopadhyay, S.; Maiti, D.; Chatterjee, S.; Devi, P.S.; Kumar, G.S. Design and application of Au decorated ZnO/TiO₂ as a stable photocatalyst for wide spectral coverage. *Phys. Chem. Chem. Phys.* **2016**, *18*, 31622–31633. [[CrossRef](#)] [[PubMed](#)]

22. Francisco, A.C.; Gustavo, C.; Ana, B.; Ricardo, S.S. Synthesis and Characterization of a ZnO/CuO/Ag Composite and its Application as a Photocatalyst for Methyl Orange Degradation. *Int. J. Electrochem. Sci.* **2018**, *13*, 9242–9256.
23. Tsai, C.-E.; Yeh, S.-M.; Chen, C.-H.; Lin, H.-N. Flexible photocatalytic paper with Cu₂O and Ag nanoparticle-decorated ZnO nanorods for visible light photodegradation of organic dye. *Nanoscale Res. Lett.* **2019**, *14*, 204. [[CrossRef](#)] [[PubMed](#)]
24. Ren, A.; Wang, B.; Zhang, H.; Ding, P.; Wang, Q. Sandwiched ZnO@Au@Cu₂O Nanorod Films as Efficient Visible-Light-Driven Plasmonic Photocatalysts. *ACS Appl. Mater. Interfaces* **2015**, *7*, 4066–4074. [[CrossRef](#)]
25. Subash, B.; Krishnakumar, B.; Swaminathan, M.; Shanthi, M. ZnS—Ag—ZnO as an excellent UV-light-active photocatalyst for the degradation of AV 7, AB 1, RR 120, and RY 84 dyes: Synthesis, characterization, and catalytic applications. *Ind. Eng. Chem. Res.* **2014**, *53*, 12953–12963. [[CrossRef](#)]
26. Gavade, N.L.; Babar, S.B.; Kadam, A.N.; Gophane, A.; Garadka, K.M. Fabrication of M@Cu_xO/ZnO (M = Ag, Au) heterostructured nanocomposite with enhanced photocatalytic performance under sunlight. *Ind. Eng. Chem. Res.* **2017**, *56*, 14489–14501. [[CrossRef](#)]
27. Kumar, S.; Saralch, S.; Pathak, D. Low-cost deposition of cupric oxide thin films for optoelectronic applications. *Eur. Phys. J. Appl. Phys.* **2018**, *84*, 20301.
28. Lin, J.; Yao, C.; Wu, L.; Jiang, K.; Hu, Z.; Li, L.; Xu, N.; Sun, J.; Wu, J. CuO: Synthesis in a highly excited oxygen-copper plasma and decoration of ZnO nanorods for enhanced photocatalysis. *J. Phys. Chem. C* **2021**, *125*, 9119–9128. [[CrossRef](#)]
29. Xu, H.; Fang, W.; Xu, L.; Liu, F. Batch preparation of CuO/ZnO-loaded nanofiber membranes for photocatalytic degradation of organic dyes. *Langmuir* **2020**, *36*, 14189–14202. [[CrossRef](#)]
30. Naseri, A.; Samadi, M.; Mohammad, N.; Pourjavadi, A.; Mehdipour, H.; Moshfegh, A.Z. Tuning composition of electrospun ZnO/CuO nanofibers: Toward controllable and efficient solar photocatalytic degradation of organic pollutants. *J. Phys. Chem. C* **2017**, *121*, 3327–3338. [[CrossRef](#)]
31. Sapkota, B.B.; Mishra, S.R. A simple ball milling method for the preparation of p-CuO/n-ZnO nanocomposite photocatalysts with high photocatalytic activity. *J. Nanosci. Nanotechnol.* **2013**, *13*, 6588–6596. [[CrossRef](#)]
32. Yuan, X.; Pei, F.; Luo, X.; Hu, H.; Qian, H.; Wen, P.; Miao, K.; Guo, S.; Wang, W.; Feng, G. Fabrication of ZnO/Au@Cu₂O heterojunction towards deeply oxidative photodegradation of organic dyes. *Sep. Purif. Technol.* **2021**, *262*, 118301. [[CrossRef](#)]
33. Vlad, I.E.; Marisca, O.T.; Vulpoi, A.; Simon, S.; Leopold, N.; Anghel, S.D. Simple approach for gold nanoparticle synthesis using an Ar-bubbled plasma setup. *J. Nanopart. Res.* **2014**, *16*, 2633. [[CrossRef](#)]
34. Ni, Y.; Sun, Z.; Zeng, Z.; Liu, F.; Qin, J. Hydrothermal fabrication of hierarchical CuO nanoflowers for dual-function amperometric sensing of hydrogen peroxide and glucose. *New J. Chem.* **2019**, *43*, 18629–18636. [[CrossRef](#)]
35. Pal, J.; Ganguly, M.; Dutta, S.; Mondal, C.; Negishi, Y.; Pal, T. Hierarchical Au-CuO Nanocomposite from Redox Transformation Reaction for Surface Enhanced Raman Scattering and Clock Reaction. *CrystEngComm* **2014**, *16*, 883–893. [[CrossRef](#)]
36. Nishino, F.; Jeem, M.; Zhang, L.; Okamoto, K.; Okabe, S.; Watanabe, S. Formation of CuO nano-flowered surfaces via submerged photo-synthesis of crystallites and their antimicrobial activity. *Sci. Rep.* **2017**, *7*, 1063. [[CrossRef](#)]
37. Mahardika, T.; Putri, N.A.; Putri, A.P.; Fauzia, V.; Roza, L.; Sugihartono, I.; Herbani, Y. Rapid and low temperature synthesis of Ag nanoparticles on the ZnO nanorods for photocatalytic activity improvement. *Results Phys.* **2019**, *13*, 102209. [[CrossRef](#)]
38. Yu, J.; Zhuang, S.; Xu, X.; Zhu, W.; Feng, B.; Hu, J. Photogenerated electron reservoir in hetero-p-n CuO-ZnO nanocomposite device for visible-light-driven photocatalytic reduction of aqueous Cr(vi). *J. Mater. Chem. A* **2015**, *3*, 1199–1207. [[CrossRef](#)]
39. Reynolds, D.C.; Look, D.C.; Jogai, B.; Litton, C.W.; Cantwell, G.; Harsch, W.C. Valence-band ordering in ZnO. *Phys. Rev. B* **1999**, *60*, 2340–2344. [[CrossRef](#)]
40. Zheng, K.; Zhang, Z.; Wang, X.; Zhan, R.; Chen, H.; Deng, S.; Xu, N.; Chen, J. Mechanism of photoluminescence quenching in visible and ultraviolet emissions of ZnO nanowires decorated with gold nanoparticles. *Jpn. J. Appl. Phys.* **2019**, *58*, 051005. [[CrossRef](#)]
41. Choudhary, M.K.; Kataria, J.; Bhardwaj, V.K.; Sharma, S. Green biomimetic preparation of efficient Ag-ZnO heterojunctions with excellent photocatalytic performance under solar light irradiation: A novel biogenic-deposition-precipitation approach. *Nanoscale Adv.* **2019**, *1*, 1035–1044. [[CrossRef](#)]
42. Wu, H.-Y.; Jian, W.-J.; Dang, H.-F.; Zhao, X.-F.; Zhang, L.-Z.; Li, J.-H. Hierarchical Ag-ZnO Microspheres with Enhanced Photocatalytic Degradation Activities. *Pol. J. Environ. Stud.* **2017**, *26*, 871–880. [[CrossRef](#)]
43. Mo, L.; Guo, Z.; Yang, L.; Zhang, Q.; Fang, Y.; Xin, Z.; Chen, Z.; Hu, K.; Han, L.; Li, L. Silver Nanoparticles Based Ink with Moderate Sintering in Flexible and Printed Electronics. *Int. J. Mol. Sci.* **2019**, *20*, 2124. [[CrossRef](#)] [[PubMed](#)]
44. Munawar, T.; Yasmeen, S.; Hussain, F.; Mahmood, K.; Hussain, A.; Asghar, M.; Iqbal, F. Synthesis of novel heterostructured ZnO-CdO-CuO nanocomposite: Characterization and enhanced sunlight driven photocatalytic activity. *Mater. Chem. Phys.* **2020**, *29*, 122983. [[CrossRef](#)]
45. Zihan, Z.; Feng, G.; Zhonghao, X.; Xiaoxuan, D.; Quian, Z. Photocatalytic degradation of an organophosphorus pesticide using a ZnO/rGO composite. *RSC Adv.* **2020**, *10*, 11929–11938.
46. Hongyu, M.; Caixia, S.; Yanhong, Z.; Bo, Z.; Debao, W. Design and synthesis of porous Ag/ZnO nanosheets assemblies as super photocatalysts for enhanced visible-light degradation of 4-nitrophenol and hydrogen evolution. *Appl. Catal. B Environ.* **2018**, *221*, 565–573.
47. Hu, W.; Zhang, Q.; Luo, K.; Yuan, H.; Li, J.; Xu, M.; Xu, S. Enhanced photocatalytic properties of CuO-ZnO nanocomposites by decoration with Ag nanoparticles. *Ceram. Int.* **2020**, *46*, 24753–24757. [[CrossRef](#)]

48. Emily, A.; Emma, K.A.; Eftihia, B.; Jonathon, A.B. CuO enhances the photocatalytic activity of Fe₂O₃ through synergistic reactive oxygen species interactions. *Colloids Surf. A Physicochem. Eng. Asp.* **2020**, *603*, 125179–125202.
49. Ren, S.; Zhao, G.; Wang, Y.; Wang, B.; Wang, Q. Enhanced photocatalytic performance of sandwiched ZnO@Ag@Cu₂O nanorod films: The distinct role of Ag NPs in the visible light and UV region. *Nanotechnology* **2015**, *26*, 125403. [[CrossRef](#)]